评述

格子 Boltzmann 方法及其在高强度聚焦超声声场建模的应用

单锋[1], 薛洪惠[1], 郭霞生[1], 屠娟[1], 章东[1,2*]

1. 南京大学声学研究所, 南京 210093;
2. 中国科学院声学研究所, 北京 100190
* 联系人, E-mail: dzhang@nju.edu.cn

摘要 格子Boltzmann方法(lattice Boltzmann method, LBM)是一种新型的流体力学模拟工具. 基于介观动力学理论, LBM具有物理意义清晰、程序易于实施、边界易于处理和并行性能好等优势, 因而在许多传统方法难以胜任的复杂流动领域得到了广泛应用. 本文首先综述了LBM的诞生、发展以及现况, 并阐述了LBM的理论和基本模型; 随后, 介绍了LBM在高强度聚焦超声(high-intensity focused ultrasound, HIFU)领域中的相关应用. 基于LBM基本模型, 构建了一种轴对称多弛豫时间(axisymmetric multiple-relaxation-time, AMRT)模型, 并在模型中采用了具有二阶精度的Bouzidi-Firdaouss-Lallemand (BFL)边界处理格式. 利用AMRT模拟了常见球面聚焦换能器产生的行波聚焦声场, 并与传统声学方法进行了对比, 验证了AMRT模型的有效性; 随后又模拟了一种新型的球腔聚焦换能器产生的驻波聚焦声场, 探讨了该类型换能器在HIFU治疗中的应用价值. 本文结果旨在推动LBM成为一种全新的有效的声学仿真手段.

关键词 格子 Boltzmann 方法, 高强度聚焦超声, 声场仿真, 亚波长焦域

格子Boltzmann方法(lattice Boltzmann method, LBM)是一种介观尺度的计算流体力学(computational fluid dynamics, CFD)方法. 区别于传统CFD方法数值求解宏观守恒方程, LBM将流体视为大量介观粒子构成的离散系统, 这些虚构的粒子沿着划分好的空间网格发生迁移和碰撞, 由局部粒子分布函数来描述粒子在格点上的分布状态, 分布函数随时间的演化则受格子Boltzmann方程(lattice Boltzmann equation, LBE)控制, 而流体的宏观状态则通过分布函数的特性统计平均获得. LBM能够通过构造相对简单的程序来真实反映流体流动的物理机制, 因而自其诞生起就得到了学术界的广泛关注和长足发展. 1988

年McNamara和Zanetti[1]首次提出采用LBE来描述分布函数的演化, 得到了最初的LBM模型; 一年后, Higuera和Jiménez[2]对该模型进行了修正, 提升了其计算效率; Chen等人[3]和Qian等人[4]分别在1991和1992年从不同角度提出了单弛豫时间(single-relaxation-time, SRT)模型; 不久之后, d'Humières[5]提出了多弛豫时间(multiple-relaxation-time, MRT)模型. 相较于SRT模型, 尽管MRT模型的计算量略有增加, 但其在数值稳定性、模型灵活度以及适用性方面具有显著的优势[6]. SRT模型和MRT模型是两种基本的LBM模型, 由此LBM进入了快速发展的时期. 1996年Sterling和Chen[7]探讨了LBM的数值稳定性问题; 同

年, Maier等人[8]研究了LBM中的边界处理格式; 1997年Abe等人[9~11]分别撰文指出LBE是连续Boltzmann方程的一种特殊离散格式, 由此揭示了LBM与经典气体动理论的内在联系. 以上工作为新LBM模型的提出搭建了理论框架. 为了模拟包含换热的流动过程, 学者们提出了多种具有不同形式的双分布函数(double-distribution-function, DDF)模型[12~14]; 为了描述流体可压缩性, 多离散速度模型[15~18]、多能级模型[19~21]以及耦合DDF模型[22]也相继出现; 为了描述包含多组分和多相态的流动过程, 陆续诞生了颜色梯度模型[23]、伪势模型[24]以及自由能模型[25]等多相流LBM模型; 此外, 研究者们也设计了一系列非标准网格LBM模型, 包括差值模型[26]、有限差分模型[27]、有限容积模型[28]、有限元模型[29]等, 此类模型的计算效率、灵活性以及适用性得到了显著提升. 相较于传统CFD方法, LBM具有物理意义清晰、程序易于实施、数值稳定性良好以及并行性能出色等显著优势[30], 因而在多组分多相流[31~33]、微纳米尺度流[34~36]、多孔介质流[37~39]、粒子悬浮流[40~42]、血液流[43~45]、湍流[46~48]等诸多传统方法难以适用的复杂流动领域得到了广泛应用. 近年来, LBM也被用于解决一些声学领域的问题, 如声流[49,50]、声吸收[51~53]、声阻抗[54~56]、声辐射力[57,58]、声波传播[59~61]等, 但传统流体力学领域仍然是LBM应用的主场.

本文首先就LBM相关的基本理论作简要阐述, 展示了SRT模型和MRT模型两种基本的LBM模型, 并介绍了一种振动曲面边界处理格式以及单位转换方法; 其后, 本文将LBM应用于高强度聚焦超声(high-intensity focused ultrasound, HIFU)中的声场仿真问题. 通过构建轴对称多弛豫时间(axisymmetric multiple-relaxation-time, AMRT)模型, 分别模拟了常见球面聚焦换能器和新型球腔聚焦换能器产生的声场, 验证了AMRT模型用于声场仿真的有效性, 并探讨了球腔聚焦换能器在HIFU治疗中的应用价值.

1 格子Boltzmann方法理论和模型

1.1 格子Boltzmann方程

LBM采用局部分布函数描述粒子在网格格点上的分布状态, 分布函数随时间的演化受LBE控制. 因此, LBM也可以被视为连续Boltzmann方程一种特殊的离散求解方式[9]. 连续Boltzmann方程描述了非平

衡态热力学系统的统计行为, 它不关注流体中单个粒子的位置$\boldsymbol{r}$和速度$\boldsymbol{v}$, 而是分析粒子处于某一状态(位置和动量)下的概率分布. 记局部分布函数为f, 粒子质量为m, 作用于流体的外力为$\boldsymbol{F}$, 连续Boltzmann方程可写为

$$\frac{\partial f}{\partial t} + \boldsymbol{v} \cdot \frac{\partial f}{\partial \boldsymbol{r}} + \boldsymbol{a} \cdot \frac{\partial f}{\partial \boldsymbol{v}} = \left(\frac{\partial f}{\partial t}\right)_{\text{coll}}, \tag{1}$$

式中, $\boldsymbol{a}=\boldsymbol{F}/m$, t为时间. 等号右侧项代表了因粒子碰撞导致的分布函数变化, 被称为碰撞项. 求解式(1)的主要难点在于形式复杂的碰撞项, 通常需要对其进行简化. 著名的Bhatnagar-Gross-Krook (BGK)近似[4]将碰撞的效果视为驱使分布函数从非平衡态向平衡态演化, 该过程中分布函数的变化率反比于两次碰撞的平均时间间隔, 即弛豫时间τ. 由此将式(1)改写为

$$\frac{\partial f}{\partial t} + \boldsymbol{v} \cdot \frac{\partial f}{\partial \boldsymbol{r}} + \boldsymbol{a} \cdot \frac{\partial f}{\partial \boldsymbol{v}} = -\frac{1}{\tau}\left(f - f^{\text{eq}}\right), \tag{2}$$

式中, f^{eq}为Maxwell平衡态分布函数

$$f^{\text{eq}} = \frac{\rho}{(2\pi RT)^{3/2}} \exp\left[-\frac{(\boldsymbol{v}-\boldsymbol{u})^2}{2RT}\right], \tag{3}$$

ρ为流体密度, $\boldsymbol{u}$为流体的宏观流动速度, R为气体常数, T为温度.

式(2)的离散化可在不同形式空间网格上进行. DnQm网格是一种常用的网格划分方式[4], 其中n代表空间维度, m代表相应的离散速度数目. 在离散速度$\boldsymbol{e} = (\boldsymbol{e}_0, \boldsymbol{e}_1, \cdots, \boldsymbol{e}_{m-1})^{\text{T}}$构成的速度空间内, 分布函数和平衡态分布函数分别可记为$\boldsymbol{f} = (f_0, f_1, \cdots, f_{m-1})^{\text{T}}$和$\boldsymbol{f}^{\text{eq}} = (f_0^{\text{eq}}, f_1^{\text{eq}}, \cdots, f_{m-1}^{\text{eq}})^{\text{T}}$. 简化起见, 不考虑外力$\boldsymbol{F}$, 式(2)可在速度空间内被离散为如下形式:

$$\begin{aligned} f_\alpha(\boldsymbol{r}+\mathrm{d}\boldsymbol{r}, t+\mathrm{d}t) &- f_\alpha(\boldsymbol{r},t) \\ &= -\frac{1}{\tau_0}\left[f_\alpha(\boldsymbol{r},t) - f_\alpha^{\text{eq}}(\boldsymbol{r},t)\right], \end{aligned} \tag{4}$$

式中, 下标α取0~$m-1$, dt和d$\boldsymbol{r}$分别为离散的时间和空间步长, $\tau_0 = \tau/\mathrm{d}t$为无量纲的弛豫时间. 式(4)即为不考虑外力的LBE, 该方程反映了分布函数随时间演化的规律, 因而也被称为控制方程.

1.2 格子Boltzmann方法基本模型

一个完备的LBM模型应该包含三个主要部件,

即离散速度(网格类型)、平衡态分布函数以及控制方程. 本文采用D2Q9网格, 这是一种二维九离散速度的正方网格, 对应的离散速度可以写为

$$\boldsymbol{e}_\alpha = \begin{bmatrix} 0 & 1 & 0 & -1 & 0 & 1 & -1 & -1 & 1 \\ 0 & 0 & 1 & 0 & -1 & 1 & 1 & -1 & -1 \end{bmatrix}, \quad (5)$$

同时, 在D2Q9网格的框架下对式(3)进行Taylor展开能够得到如下二阶精度的平衡态分布函数:

$$f_\alpha^{\mathrm{eq}} = \rho w_\alpha \left[1 + \frac{\boldsymbol{e}_\alpha \cdot \boldsymbol{u}}{c_\mathrm{s}^2} + \frac{1}{2} \left(\frac{\boldsymbol{e}_\alpha \cdot \boldsymbol{u}}{c_\mathrm{s}^2} \right)^2 - \frac{\boldsymbol{u}^2}{2c_\mathrm{s}^2} \right], \quad (6)$$

式中, $c_\mathrm{s} = \sqrt{1/3}$ 为格子声速, $w_\alpha = w\left(\left| \boldsymbol{e}_\alpha \right|^2 \right)$ 是与 $\left| \boldsymbol{e}_\alpha \right|^2$ 相关的权系数, 且有 $w(0)=4/9$, $w(1)=1/9$, $w(2)=1/36$. 此外, 控制方程可以写为

$$f_\alpha \left(\boldsymbol{r} + \boldsymbol{e}_\alpha \mathrm{d}t, t + \mathrm{d}t \right) - f_\alpha \left(\boldsymbol{r}, t \right)$$
$$= -\frac{1}{\tau_\nu} \left[f_\alpha \left(\boldsymbol{r}, t \right) - f_\alpha^{\mathrm{eq}} \left(\boldsymbol{r}, t \right) \right]. \quad (7)$$

注意到式(7)中仅包含一个弛豫时间 τ_ν, 因而由式(5)~(7)构成的LBM模型被称为SRT模型. 如前所述, 流体的宏观特征是分布函数的特性平均, 由此定义LBM模型中流体的宏观密度、动量和压强分别如下:

$$\rho = \sum_\alpha f_\alpha, \quad \rho \boldsymbol{u} = \sum_\alpha f_\alpha \boldsymbol{e}_\alpha, \quad p = \rho c_\mathrm{s}^2. \quad (8)$$

多尺度Chapman-Enskog展开[30]是一种动理学多尺度分析方法, 能够将LBM模型恢复到其对应的宏观流动方程. 利用Chapman-Enskog展开可得低Mach数下SRT模型所对应的宏观Navier-Stokes方程为

$$\frac{\partial (\rho \boldsymbol{u})}{\partial t} + \nabla \cdot (\rho \boldsymbol{u} \boldsymbol{u})$$
$$= -\nabla p + \nabla \cdot \left\{ \rho \nu \left[\nabla \boldsymbol{u} + (\nabla \boldsymbol{u})^\mathrm{T} \right] \right\}, \quad (9)$$

式中, ν 为运动黏度, 且有

$$\nu = \left(\tau_\nu - 0.5 \right) c_\mathrm{s}^2 \mathrm{d}t. \quad (10)$$

MRT模型与SRT模型基本类似, 不同之处在于MRT模型的控制方程包含了多个弛豫时间, 其形式如下:

$$f_\alpha \left(\boldsymbol{r} + \boldsymbol{e}_\alpha \mathrm{d}t, t + \mathrm{d}t \right) - f_\alpha \left(\boldsymbol{r}, t \right)$$
$$= -\sum_\beta \overline{\Lambda}_{\alpha\beta} \left[f_\beta \left(\boldsymbol{r}, t \right) - f_\beta^{\mathrm{eq}} \left(\boldsymbol{r}, t \right) \right], \quad (11)$$

式中 $\overline{\boldsymbol{\Lambda}}$ 为碰撞矩阵

$$\overline{\boldsymbol{\Lambda}} = \boldsymbol{M}^{-1} \cdot \boldsymbol{\Lambda} \cdot \boldsymbol{M}, \quad (12)$$

$\boldsymbol{M}$ 为正交矩阵

$$\boldsymbol{M} = \begin{pmatrix} 1 & 1 & 1 & 1 & 1 & 1 & 1 & 1 & 1 \\ -4 & -1 & -1 & -1 & -1 & 2 & 2 & 2 & 2 \\ 4 & -2 & -2 & -2 & -2 & 1 & 1 & 1 & 1 \\ 0 & 1 & 0 & -1 & 0 & 1 & -1 & -1 & 1 \\ 0 & -2 & 0 & 2 & 0 & 1 & -1 & -1 & 1 \\ 0 & 0 & 1 & 0 & -1 & 1 & 1 & -1 & -1 \\ 0 & 0 & -2 & 0 & 2 & 1 & 1 & -1 & -1 \\ 0 & 1 & -1 & 1 & -1 & 0 & 0 & 0 & 0 \\ 0 & 0 & 0 & 0 & 0 & 1 & -1 & 1 & -1 \end{pmatrix}, \quad (13)$$

$\boldsymbol{\Lambda}$ 为对角矩阵

$$\boldsymbol{\Lambda} = \mathrm{diag}\left(\tau_\rho^{-1}, \tau_e^{-1}, \tau_\zeta^{-1}, \tau_j^{-1}, \tau_q^{-1}, \tau_j^{-1}, \tau_q^{-1}, \tau_\nu^{-1}, \tau_\nu^{-1} \right), \quad (14)$$

且其对角元素均为弛豫时间.

将 $\boldsymbol{M}$ 用作变换矩阵能够将 $\boldsymbol{f}$ 和 $\boldsymbol{f}^{\mathrm{eq}}$ 按如下方式从速度空间投影至矩空间:

$$\boldsymbol{\Phi} = \boldsymbol{M} \cdot \boldsymbol{f}, \quad \boldsymbol{\Phi}^{\mathrm{eq}} = \boldsymbol{M} \cdot \boldsymbol{f}^{\mathrm{eq}}, \quad (15)$$

式中, $\boldsymbol{\Phi}$ 和 $\boldsymbol{\Phi}^{\mathrm{eq}}$ 分别为矩空间中的分布函数矩和平衡态分布函数矩. 进一步在式(11)中的每项左侧乘以 $\boldsymbol{M}$ 能够得到矩空间中的控制方程

$$\boldsymbol{\Phi}\left(\boldsymbol{r} + \boldsymbol{e}_\alpha \mathrm{d}t, t + \mathrm{d}t \right) = \boldsymbol{\Phi}\left(\boldsymbol{r}, t \right) - \boldsymbol{\Lambda} \cdot \left[\boldsymbol{\Phi}\left(\boldsymbol{r}, t \right) - \boldsymbol{\Phi}^{\mathrm{eq}}\left(\boldsymbol{r}, t \right) \right]. \quad (16)$$

利用多尺度Chapman-Enskog展开方法可以恢复出MRT模型所对应的宏观Navier-Stokes方程为

$$\frac{\partial (\rho \boldsymbol{u})}{\partial t} + \nabla \cdot (\rho \boldsymbol{u} \boldsymbol{u})$$
$$= -\nabla p + \nabla \cdot \left[2\mu \left(\boldsymbol{S} - \frac{1}{3} \mathrm{tr}\boldsymbol{S} \right) + \zeta \left(\nabla \cdot \boldsymbol{u} \right) \boldsymbol{I} \right], \quad (17)$$

式中, $S_{ij} = \left(\partial u_i / \partial r_j + \partial u_j / \partial r_i \right)/2$, $\mathrm{tr}\boldsymbol{S}$ 为矩阵 $\boldsymbol{S}$ 的迹, $\boldsymbol{I}$ 为单位张量, μ 和 ζ 分别为动力黏度和体黏度

$$\mu = \left(\tau_\nu - 0.5 \right) \rho c_\mathrm{s}^2 \mathrm{d}t, \quad \zeta = \left(\tau_e - 0.5 \right) \rho c_\mathrm{s}^2 \mathrm{d}t, \quad (18)$$

注意动力黏度与运动黏度的关系为 $\mu = \rho \nu$.

由于式(16)涉及矩阵运算, MRT模型的计算量相较于SRT模型增长了约15%[62], 但通过对多弛豫时间的调节能够实现模型的性能优化, 使得MRT模型能够解决某些SRT模型难以适用的流动问题[6].

1.3 边界处理格式和单位转换

Skordos指出边界处理格式的选取对LBM模型的计算精度和数值稳定性具有重要影响[63]. 这里要介绍两种精度较高的边界处理格式. 非平衡外推格式是一种适用于平直边界的外推式处理格式, 其处理方法是将边界格点上的分布函数分解为平衡态和非平衡态两部分. 记 B 为一边界格点, F 为相邻的流体格点, 迁移

过程后分布函数$f_{2,5,6}(\boldsymbol{r}_B)$未知, 将其拆分为两部分

$$f_{2,5,6}(\boldsymbol{r}_B) = f_{2,5,6}^{eq}(\boldsymbol{r}_B) + f_{2,5,6}^{neq}(\boldsymbol{r}_B), \tag{19}$$

式中, 等号右侧第一项为平衡态部分, 可以利用格点B上的宏观物理量直接求的, 若格点B上存在未知物理量, 则由格点F的相应值代替; 等号右侧第二项为平衡态部分, 可以使用外推方法得到. 考虑到格点F的分布函数$f_\alpha(\boldsymbol{r}_F)$和宏观物理量均为已知, 因此格点$B$的非平衡部分可用相邻流体格点$F$的非平衡态部分代替, 从而可得格点$B$未知的分布函数为

$$f_{2,5,6}(\boldsymbol{r}_B) = f_{2,5,6}^{eq}(\boldsymbol{r}_B) + \left[f_{2,5,6}(\boldsymbol{r}_F) - f_{2,5,6}^{eq}(\boldsymbol{r}_F)\right]. \tag{20}$$

BFL格式[64]是一种适用于曲面边界的动力学处理格式, 记某一由流体指向边界的方向为α, 格点F为靠近曲面边界的流体格点, 格点F', B和S分别为α方向上邻近格点F的内侧流体格点、实际边界格点以及外侧固体格点. BFL格式通过判断系数$q_\alpha = |\boldsymbol{r}_F - \boldsymbol{r}_B| / |\boldsymbol{r}_F - \boldsymbol{r}_S|$的值来确定格点$F$上未知分布函数的计算方式

$$
\begin{aligned}
&f_{\bar{\alpha}}^c(\boldsymbol{r}_F, t + dt)\\
&= \begin{cases}
2q_\alpha f_\alpha^c(\boldsymbol{r}_F, t) + (1 - 2q_\alpha) f_\alpha^c(\boldsymbol{r}_{F'}, t) + 6w_\alpha \boldsymbol{e}_\alpha \cdot \boldsymbol{u}_b, \\
\qquad q_\alpha < 0.5, \\
\dfrac{1}{2q_\alpha} f_\alpha^c(\boldsymbol{r}_F, t) + \left(1 - \dfrac{1}{2q_\alpha}\right) f_{\bar{\alpha}}^c(\boldsymbol{r}_F, t) + \dfrac{3}{q_\alpha} w_\alpha \boldsymbol{e}_\alpha \cdot \boldsymbol{u}_b, \\
\qquad q_\alpha \geqslant 0.5,
\end{cases}
\end{aligned}
\tag{21}
$$

式中, $\bar{\alpha}$为α的反方向, 上标c代表位于碰撞和迁移过程之前的时刻, $|\boldsymbol{r}_F - \boldsymbol{r}_B|$为格点$F$和$B$的间距, $|\boldsymbol{r}_F - \boldsymbol{r}_S|$为格点$F$和$S$的间距. $q_\alpha < 0.5$表明格点F离格点B更近, $q_\alpha \geqslant 0.5$则表明格点B离格点S更近. 此外, $\boldsymbol{u}_b$为曲面边界的运动速度, 式(21)等号右侧最后一项代表流体与曲面边界的相互作用.

LBM中所有计算均在格子单位下进行. 记A为一物理量, A^{PU}和A^{LU}分别为A在实际物理单位(physical units, PU)和格子单位(lattice units, LU)下的数值, 定义比例系数$A^{SF} = A^{PU}/A^{LU}$, 若确定A^{SF}的值即可实现物理单位和格子单位的相互转换. 根据量纲分析方法, 可得到速度u、长度l、时间t、密度ρ以及压强p对应的比例系数分别为

$$u^{SF} = \frac{c_s^{PU}}{c_s^{LU}}, \quad l^{SF} = \frac{v^{PU}}{v^{LU} u^{SF}}, \quad t^{SF} = \frac{l^{SF}}{u^{SF}},$$

$$\rho^{SF} = \frac{\rho_0^{PU}}{\rho_0^{LU}}, \quad p^{SF} = \left(u^{SF}\right)^2 \rho^{SF}, \tag{22}$$

式中, ρ_0为流体静态密度. 表1给出了室温下水的一些物理参数在物理单位(国际单位制)和格子单位下的数值, 由此可计算相关物理量的比例系数.

弛豫时间τ_v的取值需要注意两点: 一方面, 根据式(10), (18)和(20)可知l^{SF}与τ_v成反比, 也即增大τ_v能够获得更为精细的网格, 从而能够捕捉到更多的流动细节, 提升结果精度, 但同时也会导致计算量的急剧增加; 另一方面, 为保证式(10)和(18)给出的黏度具有物理意义, 需满足$\tau_v > 0.5$, 而当τ_v接近0.5时LBM模型会发生数值不稳定现象[65]. 综上所述, 具体应用时应综合考虑计算精度、计算量以及数值稳定性等因素确定τ_v的取值.

2 声场的格子Boltzmann方法仿真

2.1 轴对称多弛豫时间模型

HIFU是一种新型无创靶向治疗技术[66~68], 其技术原理是利用超声聚焦换能器将超声能量集中于焦域, 从而在不损伤周围正常组织的前提下破坏焦域内的病灶. 声场仿真能够对超声聚焦换能器的焦域形态和声能强度进行评估, 从而为HIFU治疗计划的制定提供参考. 传统的声场仿真方法大多基于数值求解非线性声波动方程[69], 包括KZK (Khokhlov-Zabolotskaya-Kuznetsov)方程[70]和扁椭球声束方程(spheroidal beam equation, SBE)[71]. 本文介绍的LBM将为声场仿真提供一种全新的思路.

超声聚焦换能器产生的三维声场通常具有轴对称性, 从而能够简化为二维的流动问题. 因此, 本文基于D2Q9网格在柱坐标系中构建适用于描述轴对称流动的AMRT模型, 其中离散速度和平衡态分布函数分别如式(5)和(6)所示, 而其控制方程则为如下形式:

$$
\begin{aligned}
&f_\alpha(\boldsymbol{x} + \boldsymbol{e}_\alpha dt, t + dt) - f_\alpha(\boldsymbol{x}, t)\\
&= -(1 + m_\alpha) \sum_\beta \overline{\Lambda}_{\alpha\beta} \left[f_\beta - f_\beta^{eq} - \left(f_\beta^{eq} + \rho\kappa_2 n_\beta\right)\frac{u_r dt}{2r}\right]\\
&\quad - \left[f_\alpha^{eq} + \rho\left(\kappa_1 m_\alpha + \kappa_2 n_\alpha\right)\right]\frac{u_r dt}{r},
\end{aligned}
\tag{23}
$$

表1 室温下水的物理参数
Table 1 Some physical parameters of water at room temperature

物理参数	物理单位	格子单位
c_s	1.48×10^3 m s^{-1}	$\sqrt{1/3}$
v	1.01×10^{-6} m^2 s	取决于τ_v
ρ_0	1.0×10^3 kg m^{-3}	1.0

式中, u_r 为流动速度 $\boldsymbol{u}$ 的径向分量. $\overline{\overline{A}}$ 形式如式(12)所示, 其中 $\tau_\rho = \tau_j = 0$, $\tau_e = \tau_\zeta = 0.505$, $\tau_q = 0.588$, τ_ν 取值待定. 此外, $n_\alpha = n\left(|e_\alpha|^2\right)$ 是与 $|e_\alpha|^2$ 相关的系数, 且有 $n(0)=-4/9$, $n(1) = -1/9$, $n(2)=2/9$. κ_1, κ_1 和 m_α 定义分别如下所示:

$$\kappa_1 = \frac{3\tau_e - \tau_\nu - 1}{9(2\tau_e - 1)}, \quad \kappa_2 = \frac{\tau_e - \tau_\nu}{2\tau_e - 1}, \quad m_\alpha = (\tau_\nu - 0.5)\frac{e_{r\alpha}}{r}. \quad (24)$$

宏观流动速度、密度以及压强扰动量(声压)分别按如下公式计算:

$$\boldsymbol{u} = \frac{\sum\limits_\alpha \boldsymbol{e}_\alpha f_\alpha}{\sum\limits_\alpha f_\alpha}, \quad \rho = \frac{\sum\limits_\alpha f_\alpha}{1 + (u_r/r)(\mathrm{d}t/2)}, \quad p = \rho c_s^2 - \rho_0 c_s^2,$$
$$(25)$$

需要注意的是, 根据L′Hôpital法则: 当 $r=0$ 式(23)和(25)中的 $u_r/r=0$, 同时式(24)中的 $e_{r\alpha}/r=0$.

利用Chapman-Enskog展开可以恢复出AMRT模型所对应的宏观Navier-Stokes方程在轴对称柱坐标系中的形式为[72,73]

$$\frac{\partial(\rho u_i)}{\partial t} + \frac{\partial(\rho u_r u_j)}{\partial r_j} + \frac{\rho u_r u_i}{r}$$
$$= -\frac{\partial p}{\partial r_i} + \frac{\partial}{\partial r_j}\left[\mu\left(\frac{\partial u_i}{\partial r_j} + \frac{\partial u_j}{\partial r_i}\right)\right] + \frac{\mu}{r}\left(\frac{\partial u_r}{\partial r_i} + \frac{u_i}{r}\right)$$
$$- \frac{(2\mu u_r \delta_{rj})}{r^2} + \frac{\partial}{\partial r_i}\left[\mu'\left(\frac{\partial u_j}{\partial r_j} + \frac{u_r}{r}\right)\right], \quad (26)$$

上述表达式采用了Einstein求和约定, 且式中 i 和 j 依次指代柱坐标 r 和 z, δ_{ij} 为Kronecker函数. μ 和 μ' 分别为动力黏度和第二黏度

$$\mu = (\tau_\nu - 0.5)\rho c_s^2 \mathrm{d}t, \quad \mu' = (\tau_e - \tau_\nu)\rho c_s^2 \mathrm{d}t, \quad (27)$$

μ' 与流体在压缩膨胀过程中的能量耗散机制相关, 通常情况下可以视为0, 但对于某些包含流体可压缩性的问题需要保留[74], 如声吸收、声衰减和激波等.

常见压电换能器的工作机制是利用压电效应驱动的机械振动激发超声声波. 传统的球面聚焦换能器能够在某一频率下激发行波聚焦声场. 与此不同的是, 新型球腔聚焦换能器的内表面同时为超声声波的激励面和反射面, 因而能够在一系列频率下激发稳定的共振驻波聚焦声场, 这种换能器的聚焦性能远远优于球面聚焦换能器, 因而在HIFU治疗中具有巨大的应用前景[75]. 图1分别展示了球面聚焦换能器和球腔聚焦换能器在柱坐标系中的剖面结构, 其中 z
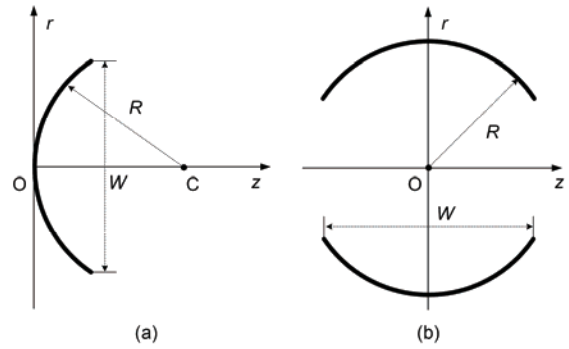

图 1 结构示意图. (a) 球面换能器; (b) 球腔换能器
Figure 1 Diagrammatic sketches. (a) Concave transducer; (b) spherical cavity transducer

轴为轴向, r 轴为径向. 图中粗线代表换能器激励面, R 为换能器曲率半径, W 为剖面长度. 为了在LBM中实现超声声波的激发, 可以在激励面上采用BFL边界处理格式, 从而可以利用AMRT模型研究这两种换能器产生的聚焦声场. 对于球面聚焦换能器, 弛豫时间取 $\tau_\nu = 0.5000235$; 对于秋抢聚焦换能器, 弛豫时间取 $\tau_\nu = 0.5000078$. 此外, 为了缩短计算耗时, 代码采用了OpenMP多线程编译处理方案.

2.2 球面聚焦换能器声场仿真

基于KZK方程的数值模型是最为常用的聚焦声场仿真工具. 受限于其近轴近似条件, KZK模型通常仅限于描述张角较小的球面聚焦换能器产生的声场. SBE模型通过在靠近声源处采用球面波近似、在远离声源处采用平面波近似, 能够较为准确地描述大张角球面聚集换能器产生的声场. 为了验证上述AMRT模型应用于声场仿真的可行性, Shan等人[76]分别采用了AMRT模型、KZK模型以及SBE模型模拟了不同张角的球面聚焦换能器产生的声场. 对于张角较小的换能器($R=5$ cm, $f=1$ MHz, $P_0=50$ kPa, $W=4$ cm), 图2(a)分别展示了利用AMRT模型和KZK模型得到的归一化轴向声压幅值分布. 由图可知, 两种模型得到的结果在焦域(本文统一取−6 dB)内较为吻合, 而在焦域外则存在轻微的差异: AMRT模型给出的近场声压幅值略微低于KZK模型的结果. 对于张角较大的换能器($R=5$ cm, $f=1$ MHz, $P_0=50$ kPa, $W=6$ cm), 图2(b)分别展示了利用AMRT模型、KZK模型和SBE模型得到的归一化轴向声压幅值分布. 由图可知, AMRT模型得到的结果在近场与SBE模型更为吻合, 而在远场两者的吻合度则并不理想, 导致这一差异的原因
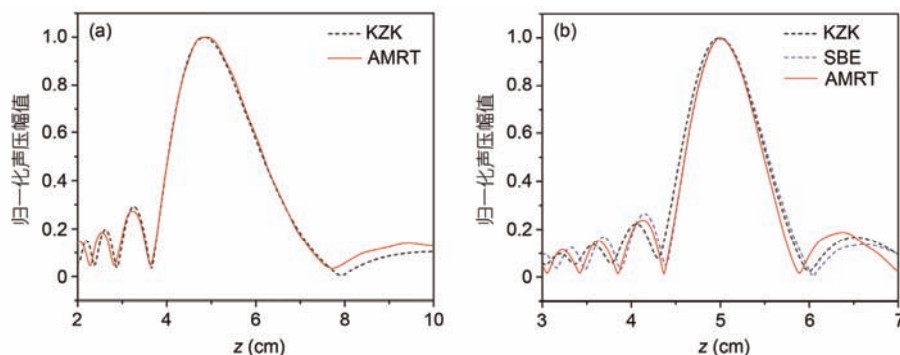
图 2 (网络版彩色)归一化轴向声压幅值分布. (a) W=4 cm; (b) W=6 cm
Figure 2 (Color online) Normalized distribution of acoustic pressure amplitude in z axis. (a) W=4 cm; (b) W=6 cm

是AMRT模型中采用的非平衡外推边界处理格式并不能完美地处理开放环境. 大量重复模拟结果表明, 尽管通过调节弛豫时间 τ_v 能够在一定程度上减小AMRT模型与SBE模型的差异, 但二者仍然在近场具有更好的吻合度. 考虑到HIFU治疗仅需关注换能器的焦域形态和声能强度, 因此可以认为AMRT模型与KZK模型和SBE模型的结果较为一致.

由如上结果可知, 球面聚焦换能器的焦域尺寸随张角增大而减小, 也即换能器聚焦性能得到了提升. 然而, 球面聚焦换能器的焦域轴向长度依然在数个波长(λ, 1 MHz下约为1.5 mm)的量级, 还不能完全满足某些高精度HIFU治疗的需求.

2.3 球腔聚焦换能器声场仿真

得益于其独特的轴对称结构, 球腔聚焦换能器能够在一系列频率上产生稳定的驻波共振聚焦声场[77]. 利用AMRT模型在420~450 kHz频率范围内对球腔聚焦换能器(R=112 mm, W=180 mm和P_0=10 kPa)的声场进行扫频模拟, 图3分别记录了AMRT模型以及实验测量给出的球腔中心(焦点)声压幅值随频率的变化. 由图可知, 球腔聚焦换能器具有一系列共振频率, 共振频率间隔约为6.6 kHz, 且共振频率的声压幅值显著高于非共振频率. AMRT模型与实验测量给出的共振频率吻合度较高, 但声压幅值却有明显差异. 尤其注意到实验测得频率422 kHz下的声压幅值远小于其他共振频率下的声压幅值, 且该频率与相邻共振频率的间隔并不为6.6 kHz, 导致这一异常的因素是多方面的, 包括实验测量精度以及换能器压电材料属性等. 后文中若无说明, 共振频率均指445.8 kHz附近.
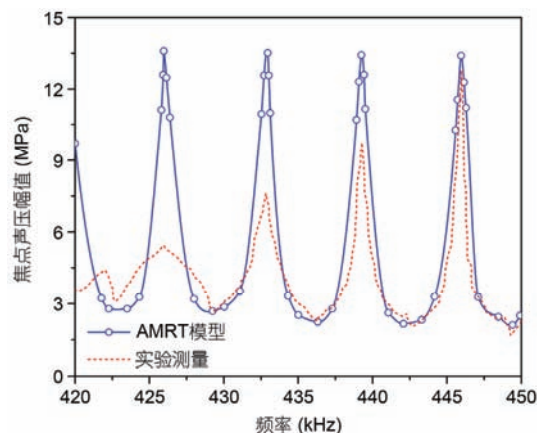

图 3 (网络版彩色)焦点声压幅值随频率变化
Figure 3 (Color online) Acoustic pressure amplitude at focus as function of frequency

图4分别展示了实验测量和AMRT模型给出的空间声压幅值分布. 由图可知, 该声场为驻波声场, 球腔中心处存在一个近椭球状的焦域, 其轴向长度略长于径向长度. 焦域两边对称分布着若干旁瓣. 焦域内声压幅值显著高于声场其他区域, 这表明球腔聚焦换能器具有出色的聚焦性能. 此外, AMRT模型和实验测量的结果吻合度较高. 理论上, 一个完整封闭的球形腔体能够形成标准的球面驻波声场, 由此表明, 球腔聚焦换能器上下两端的开口使得焦域的形状发生了轻微的畸变.

图5分别展示了AMRT模型和实验测量给出的共振频率下轴向和径向声压幅值分布. 由图可知, 焦域位于球腔几何中心处, 且焦域两边对称分布着若干旁瓣. 焦点声压幅值远高于其他位置的声压幅值, 旁瓣的声压幅值则随着远离焦点而逐渐降低. 对比图5(a)和(b)可知, 由于球腔聚焦换能器沿轴向的开口结
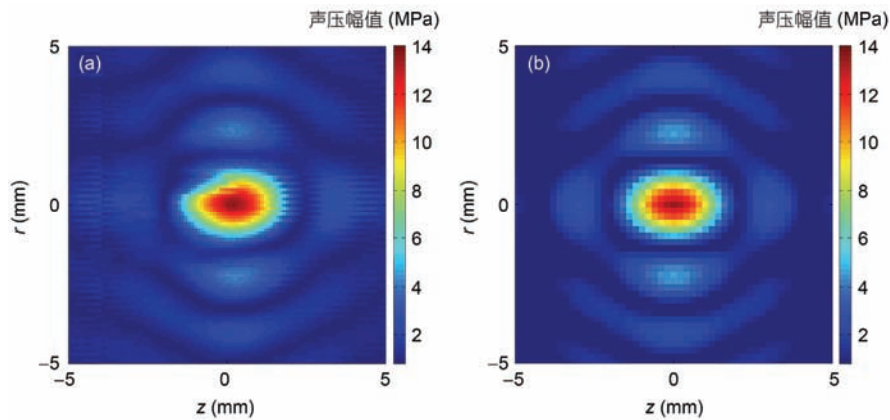
图 4 (网络版彩色)声压幅值分布. (a) 实验; (b) 模拟
Figure 4 (Color online) Distribution of acoustic pressure amplitude. (a) Experiment; (b) simulation
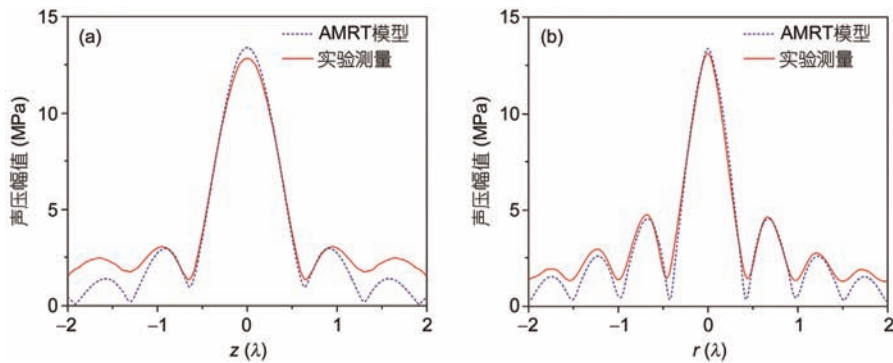

图 5 (网络版彩色)声压幅值分布. (a) 轴向; (b) 径向
Figure 5 (Color online) Distribution of acoustic pressure amplitude. (a) In z axis; (b) in r axis

构, 轴向旁瓣数目少于径向旁瓣, 且轴向旁瓣的声压幅值也较低. 整体上AMRT模型与实验测量得到的焦域吻合度较高, 在远离焦域的两端尽管旁瓣位置也相对吻合, 但旁瓣幅值却有显著差异, 且轴向的吻合度要低于径向, 其原因是AMRT模型采用的BFL格式能够较好地处理换能器振动的内表面, 但非平衡外推格式却无法理想地处理轴向开口处的开放边界. 考虑到HIFU治疗中焦域的形态和声能强度是关注的重点, 因此可以认为AMRT模型较好地描述了球腔聚焦换能器产生的驻波聚焦声场. 值得注意的是, 该球腔聚焦换能器的焦域轴、径向长度分别约为0.77λ和0.53λ(445.8 kHz下λ=3.4 mm), 均为亚波长量级, 且焦点声压幅值增益约为1300; 而利用AMRT模型计算可得相同尺寸和工作参数的普通球面聚焦换能器的焦域大小约为2.95λ×0.70λ, 且焦点声压幅值增益不到200. 对比可知, 球腔聚焦换能器的聚焦性能显著优于普通球面聚焦换能器, 因而在HIFU治疗中具有巨大的应用前景.

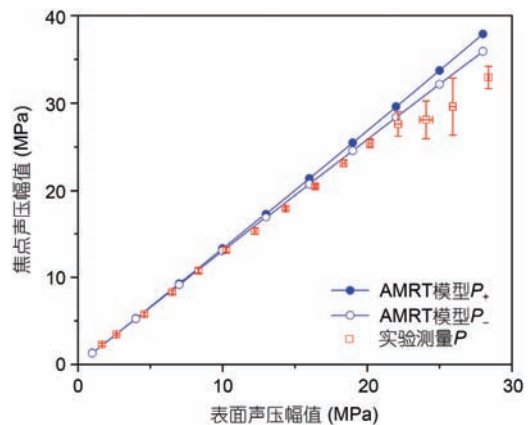图6展示了实验测量和AMRT模型给出的焦点声压幅值随表面声压幅值的变化. 由图可见, AMRT模

图 6 (网络版彩色)焦点声压幅值随表面声压幅值的变化
Figure 6 (Color online) Acoustic pressure amplitude at focus with source pressure amplitude

型得到的焦点正压幅值(P_+)和负压幅值(P_-)均随着表面声压幅值的增大而上升. 注意到P_+始终高于P_-且二者差异随着表面声压幅值逐渐增大, 这表明随着声压幅值的上升, 声场中的非线性效应越加显著. 此外, AMRT模型和实验测量的吻合度较高, 尤其在低压端. 高压端测量误差逐渐增大, 且可能伴有一定的空化现象, 因而导致实验测量与AMRT模型的结果出现了偏差.

3　结论

LBM是一种新型流体数值模拟方法, 具有物理意义清晰、程序易于实施、边界易于处理和并行性能好等优势, 能够解决传统CFD方法难以胜任的复杂流动问题. 本文首先就LBM相关的基本理论作简要阐述, 展示了SRT模型和MRT模型两种基本的LBM模型, 并介绍了BFL边界处理格式以及单位转换方法; 随后本文介绍了LBM在HIFU声场仿真领域的研究和应用; 通过构建AMRT模型并采用BFL边界处理格式, 分别模拟了普通球面聚焦换能器和新型球腔聚焦换能器产生的声场, 并与传统声学仿真方法以及实验测量进行了对比. 结果验证了AMRT模型用于声场仿真的有效性, 定量分析了球腔聚焦换能器形成的稳定驻波共振聚焦声场及其焦域, 指出了其聚焦性能显著优于普通球面聚焦换能器. 这一结果将为球腔聚焦换能器在HIFU治疗中的应用提供有力支持.

参考文献

1　McNamara G R, Zanetti G. Use of the Boltzmann equation to simulate lattice gas automata. Phys Rev Lett, 1988, 61: 2332−2335

2　Higuera F J, Jiménez J. Boltzmann approach to lattice gas simulations. Europhys Lett, 1989, 9: 663−668

3　Chen S, Chen H, Martnez D, et al. Lattice Boltzmann model for simulation of magnetohydrodynamics. Phys Rev Lett, 1991, 67: 3776−3779

4　Qian Y H, d′Humières D, Lallemand P. Lattice BGK models for the Navier-Stokes equation. Europhys Lett, 1992, 17: 479−484

5　d′Humières D. Generalized lattice-Boltzmann equations. Prog Astronaut Aeoronaut, 1994, 159: 450−458

6　Lallemand P, Luo L S. Theory of the lattice Boltzmann method: Dispersion, dissipation, isotropy, galilean invariance, and stability. Phys Rev E, 2000, 61: 6546−6562

7　Sterling J D, Chen S. Stability analysis of lattice Boltzmann methods. J Comput Phys, 1996, 123: 196−206

8　Maier R S, Bernard R S, Grunau D W. Boundary conditions for the lattice Boltzmann method. Phys Fluid, 1996, 8: 1788−1801

9　Abe T. Derivation of the lattice Boltzmann method by means of the discrete ordinate method for the boltzmann equation. J Comput Phys, 1997, 131: 241−246

10　He X, Luo L S. A priori derivation of the lattice Boltzmann equation. Phys Rev E, 1997, 55: 6333−6336

11　Shan X, He X. Discretization of the velocity space in solution of the Boltzmann equation. Phys Rev Lett, 1997, 80: 65−68

12　He X, Chen S, Doolen G D. A novel thermal model for the lattice Boltzmann method in incompressible limit. J Comput Phys, 1998, 146: 282−300

13　Guo Z, Shi B, Zheng C. A coupled lattice BGK model for the Boussinesq equations. Int J Numer Meth Fluid, 2002, 39: 325−342

14　Guo Z, Zheng C, Shi B, et al. Thermal lattice Boltzmann equation for low Mach number flows: Decoupling model. Phys Rev E, 2007, 75: 036704

15　Qian Y H. Simulating thermohydrodynamics with lattice BGK models. J Sci Comput, 1993, 8: 231−242

16　Alexander F J, Chen S, Sterling J D. Lattice Boltzmann thermohydrodynamics. Phys Rev E, 1993, 47: R2249

17　Chen Y, Ohashi H, Akiyama M. Thermal lattice BGK model without nonlinear deviations in macrodynamic equations. Phys Rev E, 1994, 50: 2776−2783

18　Chen Y, Ohashi H, Akiyama M. Two-parameter thermal lattice BGK model with a controllable Prandtl number. J Sci Comput, 1997, 12: 169−185

19　Hu S X, Yan G W, Shi W P. Lattice Boltzmann model for compressible perfect gas. Acta Mech Sin, 1997, 13: 218−226

20　Sun C. Lattice-Boltzmann models for high speed flows. Phys Rev E, 1998, 58: 7283−7287

21　Kataoka T, Tsutahara M. Lattice Boltzmann method for the compressible Euler equations. Phys Rev E, 2004, 69: 056702

22　Li Q, He Y L, Wang Y, et al. Coupled double-distribution-function lattice Boltzmann method for the compressible Navier-Stokes equations. Phys Rev E, 2007, 76: 056705

23　Gunstensen A K, Rothman D H, Zaleski S, et al. Lattice Boltzmann model of immiscible fluids. Phys Rev A, 1991, 43: 4320−4327

24 Shan X, Chen H. Lattice Boltzmann model for simulating flows with multiple phases and components. Phys Rev E, 1993, 47: 1815–1819

25 Swift M R, Osborn W R, Yeomans J M. Lattice Boltzmann simulation of nonideal fluids. Phys Rev Lett, 1995, 75: 830–833

26 He X, Luo L S, Dembo M. Some progress in lattice Boltzmann method. Part 1: Nonuniform mesh grids. J Comput Phys, 1996, 129: 357–363

27 Reider M B, Sterling J D. Accuracy of discrete-velocity BGK models for the simulation of the incompressible Navier-Stokes equations. Comput Fluid, 1995, 24: 459–467

28 Nannelli F, Succi S. The lattice Boltzmann equation on irregular lattices. J Stat Phys, 1992, 68: 401–407

29 Lee T, Lin C L. A characteristic Galerkin method for discrete Boltzmann equation. J Comput Phys, 2001, 171: 336–356

30 Chen S, Doolen G D. Lattice Boltzmann method for fluid flows. Annu Rev Fluid Mech, 2003, 30: 329–364

31 Zheng H W, Shu C, Chew Y T. A lattice Boltzmann model for multiphase flows with large density ratio. J Comput Phys, 2006, 218: 353–371

32 Huang H, Thorne D T, Schaap M G, et al. Proposed approximation for contact angles in Shan-and-Chen-type multicomponent multiphase lattice Boltzmann models. Phys Rev E, 2007, 76: 066701

33 Chen L, Kang Q, Mu Y, et al. A critical review of the pseudopotential multiphase lattice Boltzmann model: Methods and applications. Int J Heat Mass Transf, 2014, 76: 210–236

34 Zhang J. Lattice Boltzmann method for microfluidics: Models and applications. Microfluid Nanofluid, 2011, 10: 1–28

35 Fattahi E, Farhadi M, Sedighi K, et al. Lattice Boltzmann simulation of natural convection heat transfer in nanofluids. Int J Therm Sci, 2012, 52: 137–144

36 Sheikholeslami M, Gorji-Bandpy M, Ganji D D. Lattice Boltzmann method for MHD natural convection heat transfer using nanofluid. Powder Tech, 2014, 254: 82–93

37 Pan C, Luo L S, Miller C T. An evaluation of lattice Boltzmann schemes for porous medium flow simulation. Comput Fluid, 2006, 35: 898–909

38 Boek E S, Venturoli M. Lattice-Boltzmann studies of fluid flow in porous media with realistic rock geometries. Comput Math Appl, 2010, 59: 2305–2314

39 Ata A S V, Javaherdeh K, Ashorynejad H R. Magnetic field effects on force convection flow of a nanofluid in a channel partially filled with porous media using lattice Boltzmann method. Adv Powder Tech, 2014, 25: 666–675

40 Kromkamp J, Ende D V D, Kandhai D, et al. Lattice Boltzmann simulation of 2D and 3D non-Brownian suspensions in Couette flow. Chem Eng Sci, 2006, 61: 858–873

41 Švec O, Skoček J, Stang H, et al. Free surface flow of a suspension of rigid particles in a non-Newtonian fluid: A lattice Boltzmann approach. J Non-Newton Fluid Mech, 2012, 179: 32–42

42 Tan J, Keller W, Sohrabi S, et al. Characterization of nanoparticle dispersion in red blood cell suspension by the lattice Boltzmann-immersed boundary method. Nanomater, 2016, 6: 30–43

43 Ouared R, Chopard B. Lattice Boltzmann simulations of blood flow: Nonnewtonian Rheology and Clotting processes. J Stat Phys, 2005, 121: 209–221

44 Zhang J, Johnson P C, Popel A S. Red blood cell aggregation and dissociation in shear flows simulated by lattice Boltzmann method. J Biomech, 2008, 41: 47–55

45 Jr D A R, Clausen J R, Aidun C K. Coupling the lattice-Boltzmann and spectrin-link methods for the direct numerical simulation of cellular blood flow. Int J Numer Meth Fluid, 2012, 68: 767–781

46 Premnath K N, Pattison M J, Banerjee S. Generalized lattice Boltzmann equation with forcing term for computation of wall-bounded turbulent flows. Phys Rev E, 2009, 79: 026703

47 Feng Y T, Han K, Owen D R J. Coupled lattice Boltzmann method and discrete element modelling of particle transport in turbulent fluid flows: Computational issues. Int J Numer Meth Eng, 2010, 72: 1111–1134

48 Fattahia E, Waluga C, Wohlmuth B, et al. Pore-scale lattice Boltzmann simulation of laminar and turbulent flow through a sphere pack. Comput Sci, 2015, 667: 135–157

49 Haydock D, Yeomans J M. Lattice Boltzmann simulations of acoustic streaming. J Phys A, 2001, 34: 5201–5213

50 Rafat Y, Habibi K, Mongeau L. Direct numerical simulations of acoustic streaming in standing wave tubes using the lattice Boltzmann method. Proc Mtgs Acoust, 2013, 19: 045006

51 Habibi K, Lew P, Mongeau L. Prediction of sound absorption characteristics of orifice plates with mean flow using the lattice Boltzmann method. J Acoust Soc Am, 2011, 129: 2613

52 Ji C, Zhao D. Two-dimensional lattice Boltzmann investigation of sound absorption of perforated orifices with different geometric shapes. Aerosp Sci Tech, 2014, 39: 40–47

53　Habibi K, Mongeau L. Prediction of sound absorption by a circular orifice termination in a turbulent pipe flow using the lattice-Boltzmann method. Appl Acoust, 2015, 87: 153–161

54　Silva A R D, Depalle P, Scavone G. Benchmarking the lattice Boltzmann method for the determination of acoustic impedances of axisymmetric waveguides. J Acoust Soc Am, 2006, 119: 3383

55　Toutant A, Sagaut P. Lattice Boltzmann simulations of impedance tube flows. Comput Fluid, 2009, 38: 458–465

56　Guan D, Wu J H, Jing L, et al. Lattice Boltzmann simulation of acoustic resistance in microchannels. Int J Mod Phys B, 2015, 29: 1550104

57　Haydock D. Lattice Boltzmann simulations of the time-averaged forces on a cylinder in a sound field. J Phys A Gen Phys, 2005, 38: 3265–3277

58　Barrios G, Rechtman R. Dynamics of an acoustically levitated particle using the lattice Boltzmann method. J Fluid Mech, 2008, 592: 191–200

59　Huang L. A lattice Boltzmann approach to acoustic-wave propagation. Adv Geophys, 2007, 48: 517–559

60　Zhang J, Yan G, Shi X. Lattice Boltzmann model for wave propagation. Phys Rev E, Stat Nonlin Soft Matter Phys, 2009, 80: 026706

61　Viggen E M. Viscously damped acoustic waves with the lattice Boltzmann method. Philos Transact A Math Phys Eng Sci, 2011, 369: 2246–2254

62　d'Humières D, Ginzburg I, Krafczyk M, et al. Multiple-relaxation-time lattice Boltzmann models in three dimensions. Philos Trans R Soc Lond A, 2002, 360: 437–451

63　Skordos P A. Initial and boundary conditions for the lattice Boltzmann method. Phys Rev E, 1993, 48: 4823–4842

64　Bouzidi M, Firdaouss M, Lallemand P. Momentum transfer of a Boltzmann-lattice fluid with boundaries. Phys Fluid, 2001, 13: 3452–3459

65　Huang H, Lee T S, Shu C. Lattice-BGK simulation of steady flow through vascular tubes with double constrictions. Int J Numer Methods Heat Fluid Flow, 2006, 16: 185–203

66　Wu F, Wang Z B, Chen W Z, et al. Preliminary experience using high intensity focused ultrasound for the treatment of patients with advanced stage renal malignancy. J Urol, 2003, 170: 2237–2240

67　Kennedy J E, Wu F, terHaar G R, et al. High-intensity focused ultrasound for the treatment of liver tumours. Ultrasonics, 2004, 42: 931–935

68　Kennedy J E. High-intensity focused ultrasound in the treatment of solid tumours. Nat Rev Cancer, 2005, 5: 321–327

69　Xue T, Lord W, Udpa S. Numerical analysis of the radiated fields of ultrasonic transducers. J Nondestruct Eval, 1995, 14: 137–146

70　Kuznetsov V P. Equations of nonlinear acoustics. Soviet Phys Acoust, 1971, 15: 467–470

71　Tjøtta J N, Tjøtta S, Vefring E H. Effects of focusing on the nonlinear-interaction between 2 collinear finite-amplitude sound beams. J Acoust Soc Am, 1991, 89: 1017–1027

72　Wang L, Guo Z L, Zheng C G. Multi-relaxation-time lattice Boltzmann model for axisymmetric flows. Comput Fluid, 2010, 39: 1542–1548

73　Xie W J. An axisymmetric multiple-relaxation-time lattice Boltzmann scheme. J Comput Phys, 2015, 281: 55–66

74　Karim S M. Second viscosity coefficient of liquids. J Acoust Soc Am, 1954, 25: 997–1002

75　Li F Q, Wang H, Zeng D P, et al. Sub-wavelength ultrasonic therapy using a spherical cavity transducer with open ends. Appl Phys Lett, 2013, 102: 204102

76　Shan F, Guo X S, Tu J, et al Multi-relaxation-time lattice Boltzmann modeling of the acoustic field generated by focused transducer. Int J Mod Phys C, 2017, 28: 1750038

77　Shan F, Tu J, Cheng J C, et al. Acoustic field of an ultrasonic cavity resonator with two open ends: Experimental measurements and lattice Boltzmann method modeling. J Appl Phys, 2017, 121: 124502

Summary for "格子 Boltzmann 方法及其在高强度聚焦超声声场建模的应用"

Lattice Boltzmann method and its application in the modelling of high intensity focused ultrasound (HIFU)

SHAN Feng[1], XUE HongHui[1], GUO XiaSheng[1], TU Juan[1] & ZHANG Dong[1,2*]

[1] *Key Laboratory of Modern Acoustics (MOE), Nanjing University, Nanjing 210093, China;*
[2] *Institute of Acoustics, Chinese Academy of Sciences, Beijing 100190, China*
* Corresponding author, E-mail: dzhang@nju.edu.cn

High-intensity focused ultrasound (HIFU) is a breakthrough of noninvasive targeted therapeutic technique for tumor treatments. The operational procedure of HIFU is to concentrate the ultrasound energy into the focal region by using the ultrasound transducer, and the focused ultrasound energy is sufficient to rapidly rise the temperature of tumor located at the focal region up to above 65°C and locally destroy the tumor for coagulation necrosis. The ultrasound transducer is the key component in HIFU treatment to generate the high-intensity focused ultrasound energy, the dimension of focal region generated by the transducer is closely relevant to the safety of HIFU treatment. Therefore, it is necessary to simulate the acoustic field numerically for estimating the performance, optimizing the parameters and reducing the design cost of the focused ultrasound transducer. Besides, the common spherical transducer is the most widely used transducer in HIFU, but the size of its focal region still could not satisfy the requirements of some sophisticated applications. So, it is necessary to adopt some new kinds of focused ultrasound transducers with better focusing performance. Aiming at these issues, we presented a numerical simulation method called the lattice Boltzmann method (LBM) in this paper. It is a novel fluid dynamic simulation approach based on mesoscopic kinetic theory, which takes prominent advantages of distinct physical meaning, easy implementation and excellent parallel performance. The LBM has shown great potential in numerical simulations of complex flows that would be difficult for traditional methods. Firstly, we reviewed the developments and applications of the LBM. Then, we revealed the inherent relationship between the LBM and the Boltzmann equation, and presented two basic LBM models called the single-relaxation-time (SRT) model and multiple-relaxation-time (MRT) model, recovered the corresponding macroscopic Navier-Stokes equations respectively via the Chapman−Enskog expansion, presented two common boundary conditions called the non-equilibrium extrapolation scheme and the BFL scheme. Besides we introduced the conversion method between the physical units and lattice units based on dimensional analysis. After that, we built an axisymmetric multiple-relaxation-time (AMRT) LBM model with the BFL scheme, and simulated the acoustic fields generated by concave ultrasound transducers of different field angles respectively by the AMRT model, Khokhlov-Zabolotskaya-Kuznetsov (KZK) equation and spheroidal beam equation (SBE). Results indicated that the AMRT model could be used to describe the acoustic field generated by the concave ultrasound transducer, and the transducer with bigger field angle had a better focusing performance. Lastly, we presented a novel spherical cavity transducer with two open ends for providing subwavelength focal region and sufficient pressure gain. We investigated the standing wave acoustic field generated by the spherical cavity ultrasound transducer via the AMRT model and experimental measurements. Results indicated that the AMRT model could be used to describe the standing wave filed generated by the spherical cavity ultrasound transducer, and this device exhibited much better focusing performance than the traditional concave ultrasound transducer, and could meet the requirement of some sophisticated HIFU treatments. The main aim of this work is to solve some practical problems for the numerical modeling of acoustic field in the HIFU treatments and provide new sights into the acoustic simulations.

lattice Boltzmann method, high-intensity focused ultrasound, acoustic field simulation, sub-wavelength focal region